HHS Public Access

Author manuscript

*J Am Chem Soc*. Author manuscript; available in PMC 2020 January 30.

Published in final edited form as:

*J Am Chem Soc*. 2019 January 30; 141(4): 1725–1734. doi:10.1021/jacs.8b12415.

# Generalized Preparation of Two-Dimensional Quasi-nanosheets via Self-assembly of Nanoparticles

**Ren Cai**[†,§,#], **Dan Yang**[■,#], **Keng-Te Lin**[■], **Yifan Lyu**[‡,§], **Bowen Zhu**[●], **Zhen He**[§,⊥], **Lili Zhang**[†], **Yusuke Kitamura**[§], **Liping Qiu**[†], **Xigao Chen**[§], **Yuliang Zhao**[‖], **Zhuo Chen**[*,†], and **Weihong Tan**[*,†,‡,§]

[†]Molecular Science and Biomedicine Laboratory (MBL), State Key Laboratory for Chemo/Bio-Sensing and Chemometrics, College of Chemistry and Chemical Engineering, College of Biology, Aptamer Engineering Center of Hunan Province, Hunan University Changsha, Hunan 410082, China

[‡]Institute of Molecular Medicine (IMM), Renji Hospital, Shanghai Jiao Tong University School of Medicine, and College of Chemistry and Chemical Engineering, Shanghai Jiao Tong University, Shanghai, China

[§]Department of Chemistry and Department of Physiology and Functional Genomics, Center for Research at the Bio/Nano Interface, Health Cancer Center, UF Genetics Institute and McKnight Brain Institute, University of Florida, Gainesville, Florida 32611-7200, United States

[‖]CAS Key Lab for Biomedical Effects of Nanomaterials & Nanosafety, Institute of High Energy Physics, Chinese Academy of Sciences, Beijing 100049, China

[⊥]Department of Colorectal Surgery, the Sixth Affiliated Hospital, Sun Yat-sen University, 26 Yuancun Er Heng Road, Guangzhou, Guangdong 510655, China

[■]Centre for Micro-Photonics, Faculty of Science, Engineering and Technology, Swinburne University of Technology, P.O. Box 218, Hawthorn, VIC 3122, Australia

[●]School of Materials Science and Engineering, Nanyang Technological University, 50 Nanyang Avenue, Singapore 639798, Singapore

## Abstract

Two-dimensional (2D) nanomaterials are attracting increasing research interest because of their unique properties and promising applications. Here, we report a facile method to manipulate the assembly of nanoparticles (NPs) to fabricate free-standing 2D quasi-nanosheets. The as-generated 2D products are composed of few-layer NPs; that is, their thicknesses are only tens of nanometers but lateral dimensions could be up to several micrometers. Therefore, the novel structure was denoted as 2D “quasi-nanosheets (QNS)”. Specifically, several types of building blocks could be

[*]**Corresponding Authors:** tan@chem.ufl.edu zhuochen@hnu.edu.cn.
[#]These authors contributed equally to this work (R.C. and D.Y.).

The authors declare no competing financial interest.

Supporting Information

The Supporting Information is available free of charge on the ACS Publications website at DOI: 10.1021/jacs.8b12415.
Detailed experimental procedures and supplementary data (PDF)

assembled into 2D unary, binary, ternary, and even quaternary QNS by a universal procedure. The entire assembly process is carried out in solution and mediated simply by tuning the concentration of ligands surrounding the NPs. In contrast to traditional assembly techniques, even without any substrate or template, these QNS showed exceptionally high stability. They can remain intact for several days without any disassembly regardless of the solvent environment (e.g., water, ethanol, methanol, and hexane). In general, our method has effectively tackled several limitations associated with traditional assembly techniques and allows more freedom in manipulating assembly of NPs, which may hold great potential for future fabrication of 2D devices with rich functionalities.

## Graphical Abstract

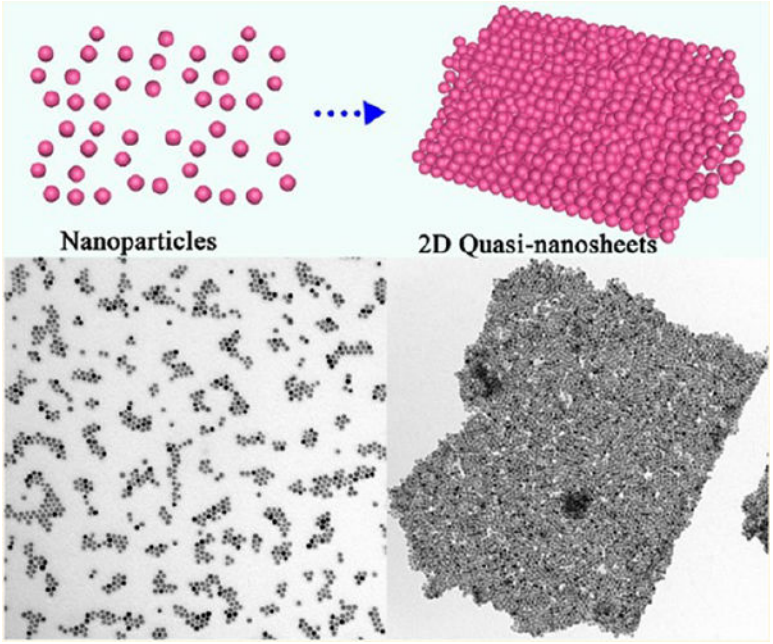


## INTRODUCTION

Programmable design of novel two-dimensional (2D) structures consisting of assembled nanoparticles (NPs) has led to various specific properties and functionalities,[1–3] as well as deep insights into the fundamental science underlying the assembly behavior of building blocks.[4,5] Particularly, 2D superlattices with ordered assembly from nanocrystals have been widely investigated in recent decades.[6,7] For example, superlattices from self-assembly of triangular gold nanoprisms bring about surface-enhanced Raman spectroscopy (SERS) enhancement relative to that of disordered assemblies.[8] Binary superlattices co-assembled by PbTe and $Ag_2Te$ NPs display higher electrical conductivity compared to each individual component (i.e., PbTe NPs or $Ag_2Te$ NPs).[9] 2 To date, fabrication of assembled 2D structures mostly relied on using block copolymers as templates,[10,11] from Langmuir–Blodgett assembly,[12] or with traditional drying-mediated processes.[13] Moreover, substrates are always necessary to transfer or preserve these mono- or multilayer 2D films,[14] which limits their independence, free mobility, and applications. So far, few effective methods have

been reported to align NPs into stable and free-standing 2D nanosheets without any additional supports.[15] In addition, manipulation of self-assembly of multiple building blocks is even more challenging than that of a single component, owing to the complexity in dealing with a number of interactions, such as van der Waals, Coulombic, and dipolar interactions, as well as hard-sphere space-filling rules.

Herein, we adopted a facile route to manipulate assembly of NPs to fabricate a new 2D structure: quasi-nanosheets (QNS). Typical QNS displayed thicknesses of a few nanometers and lateral dimensions up to several micrometers. These can be achieved simply by tuning the concentration of aliphatic ligands (e.g., 1-octadecene (ODE) present in the solution, without any substrate or template. As a universal assembly procedure, involving various NP building blocks, 2D unary, binary, ternary, and quaternary QNS were fabricated. These QNS could be freely dispersed and remain stable in both polar and nonpolar solvents for several days without any disassembly. These unique properties allow the QNS to be processed in various conditions and environments, which will be very beneficial for their future applications. As a proof of concept, excellent optical properties in the surface-enhanced Raman scattering (SERS) have been achieved from Pd–Pt QNS, indicating the synergetic advantage achieved by the assembled structure.

## EXPERIMENTAL SECTION

Synthesis of free-standing 2D unary QNS is as follows. In a typical self-assembly experiment,[16] 32 μL of octadecene (ODE) was added to a chloroform solution of 16 nm of $Fe_3O_4$ NPs (1 mg, 0.25 mL) by a vortex mixer for 30 min (Figure S1 (Supporting Information)). Then an aqueous solution of a cationic surfactant, dodecyltrimethylammonium bromide (DTAB, 150 μL, 20 mg/mL), was added to the mixture. Afterward, the mixture was heated and vigorously agitated by vortexing. Subsequently, 1 mL of mixed solvent (ethylene glycol (EG) and polyvinylpyrrolidone (PVP, 0.1 g, $M_w$ = 55 000)) was added swiftly to the emulsion and subjected to vortexing for 2 min. The emulsion was then heated to 83 °C, kept at this temperature for 120 min to evaporate the residual chloroform phase, and then held for another 1 h before the suspension was cooled to room temperature. Finally, the resulting products were washed several times with ethanol to remove impurities, followed by centrifugation at 4000 rpm for 8 min and then redispersal in ethanol prior to being characterized.

With use of the same strategy, 4, 8, 16, 24, 40, and 48 μL of ODE was used to stabilize NPs to form particle–micelles prior to the self-assembly process, separately.

For synthesis of free-standing 2D unary, binary, ternary, and quaternary QNS from $Fe_3O_4$ NPs, Pd NPs, Pt NPs, and CdSe NPs, please see the Supporting Information.

## RESULTS AND DISCUSSION

As revealed by scanning electron microscopy (SEM), vertically aligned “nanosheets” with lateral dimensions up to several micrometers were obtained (Figure 1a), and the 2D feature was confirmed by a transmission electron microscopy (TEM) image (Figure 1b). The enlarged TEM images further revealed that each “sheet” was composed of densely packed

NPs (Figure 1c,d). Therefore, the novel 2D structure was denoted as 2D “quasi-nanosheets” (QNS). The selected area (electron) diffraction (SAED) pattern showed a diffused ring pattern, which indicated the “amorphous” feature and different orientations of NPs (inset, Figure 1d). The thicknesses of typical QNS were measured to be ~53 nm by atomic force microscopy (AFM) image (Figure 1e). Importantly, as confirmed by our experiments, these QNS displayed the free-standing and stable feature when they were redispersed in various solvents and remained intact for at least 1 day (Figure S2), outperforming mono- or multilayer superlattices from solvent-induced alignment of NPs,[17,18] whose structures are unstable without substrate or supports and would be disturbed by agitation or solvent change.

Because the assembly environment involves quite a few species (e.g., PVP, EG, DTAB, and ODE), it is difficult to clarify the mechanism underlying the assembly process. To elucidate the growth mechanism of the QNS, we systematically investigated the effect of removing each individual parameter while keeping other conditions constant. For example, by removing PVP from the EG solvent, no product was collected; and when DTAB was removed, only irregular aggregates were obtained (Figure S3). Obviously, coexistence of both PVP and DTAB is a prerequisite for QNS assembly. Combined with a previously reported mechanism and our observations,[19] PVP and DTAB act as active “separators” to promote the dispersion of the NPs. On the other hand, the ligand ODE plays a more critical and delicate role to “fine-tune” the assembled structure. As shown in Figure 2a, without ODE, bare NPs easily aggregated to form irregular microparticles.[20] In contrast, with 4 μL of ODE, as-obtained products were “small” microparticles with a tendency to spread out (Figure 2b). Further increase of ODE to 8 μL induced formation of folded 2D nanosheets (Figure 2c). Finally, well-dispersed and stable QNS were generated when 24 and 32 μL of ODE were added (Figure 2d and Figure 1). Interestingly, the QNS decomposed into irregular debris when the amount of ODE was further increased to 48 μL (Figure 2e). These results demonstrate that formation of QNS closely correlates with the amount of ODE (Figure 2f).

On the basis of the above observation, we proposed a mechanism to interpret formation of the 2D QNS (Figure 3). DTAB as a cationic surfactant endows the NPs with amphiphilic properties through formation of an interdigitated bilayer structure,[21] with ODE (organic ligand) as the inner layer and DTAB as the outer layer. These are held together by van der Waals interactions between their aliphatic chains (Figure S5b).[16,22,23] With the hydrophilic structure (DTAB layer), as-prepared NP–micelles could be uniformly dispersed in mixed solvent (EG and PVP) (Figure 3a). Because the solubility of DTAB increases with temperature in the mixed solvent, the outer layer of NP–micelles (DTAB) starts to self-dissociate when the micelles are heated, leaving ODE-capped NPs wrapped inside the mixed solvent (Figure 3b), producing “microinterfaces” between mixed solvent (hydrophilic) and the ODE-capped NP aggregates (hydrophobic). $^{1}$H NMR spectra confirmed the absence of DTAB and the presence of ODE (Figure S6). Formation of such hydrophilic–hydrophobic microinterfaces could foster the subsequent self-assembly process without disruption of solvent (Figure 3c), and allow for further arrangement of NPs to form free-standing QNS (Figure 3d). In general, the process can be regarded as an approach to dynamic balance between elastic repulsive forces contributed by the ligands (ODE) and van der Waals attractive forces between the NPs during the formation of 2D QNS.[24,25] In addition, there is

also hydrophobic attraction between the NPs because ODE has hydrophobic groups.[15] However, when the van der Waals and hydrophobic attractive forces are not sufficient to balance the strong ligand elastic repulsive forces (excessive ODE was added), the as-assembled structures are no longer stable, eventually resulting in the collapse of the 2D structure into irregular debris (Figure 2e).[26] On the basis of the above mechanism, in which formation of the QNS is independent of type of original building blocks, it is reasonable to generalize this process into fabrication of new 2D QNS from assembly of different kinds of building blocks. As a demonstration, Pd, Pt, and CdSe QNS were successfully assembled by simply changing the NP building blocks in this simple bottom-up process (Figure 4).

As reported previously,[27,28] self-assembly of free-standing 2D binary QNS is still a challenge because of the lack of stable supports. Here, with similar strategy described above, we can achieve 2D binary QNS (Figure 5a) through combination of any two building blocks in our “library”, that is, $Fe_3O_4$ NPs (~16 nm), CdSe NPs (~15 nm), Pd NPs (~6 nm), and Pt NPs (~3.5 nm) (Figure S7). In detail, a binary self-assembly was initiated by adding Pd NP–micelles to a solution containing $Fe_3O_4$ NP–micelles, followed by similar processing steps (see Experimental Section in the Supporting Information). As shown in SEM and TEM images (Figure 5b,c), well-dispersed 2D QNS with lateral sizes up to several micrometers were observed. Moreover, the enlarged TEM image clearly shows that $Fe_3O_4$ NPs and Pd NPs were efficiently packed together, and displayed “amorphous” behavior in the SAED pattern (Figure 5d, inset). The thickness of one binary QNS was measured to be 44.8 nm (Figure 5e, inset), which did not increase with addition of NPs of different types. Similar to the unary QNS, these 2D binary QNS also exhibited good stability and free-floating feature in various solvents (Figure S8). Meanwhile, the density of assembled NPs in 2D binary QNS could be controlled by adjusting the relative NP ratio (Figure S9). A wide range of binary 2D QNS, for example, $Fe_3O_4$–Pt QNS, $Fe_3O_4$–CdSe QNS, CdSe–Pd QNS, CdSe–Pt QNS, and Pd–Pt QNS were successfully achieved (Figure 6). It is interesting to note that ternary QNS could be fabricated by further involving three types of NPs in the system (Figure 7a). For instance, $Fe_3O_4$ NPs, Pd NPs, and Pt NPs were easily assembled into 2D ternary QNS (Figure 7b), and each type of NPs could be clearly distinguished in the enlarged TEM image. Meanwhile, an infinite set of new 2D ternary QNS can be assembled in Figure 7c–e. All four types of NPs, although they have different sizes, were co-assembled to form free-standing 2D quaternary QNS (Figure S10).

As reported previously,[27,28] self-assembly of free-standing 2D binary QNS is still a challenge because of the lack of stable supports. Here, with strategy similar to that described above, we can achieve 2D binary QNS (Figure 5a) through combination of any two building blocks in our “library”, that is, $Fe_3O_4$ NPs (~16 nm), CdSe NPs (~15 nm), Pd NPs (~6 nm), and Pt NPs (~3.5 nm) (Figure S7). In detail, a binary self-assembly was initiated by adding Pd NP–micelles to a solution containing $Fe_3O_4$ NP–micelles, followed by similar processing steps (see Experimental Section in Supporting Information). As shown in SEM and TEM images (Figure 5b,c), well-dispersed 2D QNS with lateral sizes up to several micrometers were observed. Moreover, the enlarged TEM image clearly shows that $Fe_3O_4$ NPs and Pd NPs were efficiently packed together, and displayed “amorphous” behavior in the SAED pattern (Figure 5d, inset). The thickness of one binary QNS was measured to be 44.8 nm (Figure 5e, inset), which did not increase with addition of NPs of different types. Similar to

the unary QNS, these 2D binary QNS also exhibited good stability and free-floating feature in various solvents (Figure S8). Meanwhile, the density of assembled NPs in 2D binary QNS could be controlled by adjusting the relative NP ratio (Figure S9). A wide range of binary 2D QNS, for example, $Fe_3O_4$–Pt QNS, $Fe_3O_4$–CdSe QNS, CdSe–Pd QNS, CdSe–Pt QNS, and Pd–Pt QNS were successfully achieved (Figure 6). It is interesting to note that ternary QNS could be fabricated by further involving three types of NPs in the system (Figure 7a). For instance, $Fe_3O_4$ NPs, Pd NPs, and Pt NPs were easily assembled into 2D ternary QNS (Figure 7b), and each type of NPs could be clearly distinguished in the enlarged TEM image. Meanwhile, an infinite set of new 2D ternary QNS can be assembled in Figure 7c–e. All four types of NPs, although they have different sizes, were co-assembled to form free-standing 2D quaternary QNS (Figure S10).

With free manipulation of the composition and structure of the 2D assembly, various intriguing synergetic effects can be expected. As a proof of concept, here we investigated the optical behavior of the 2D binary Pd–Pt QNS. A three-dimensional finite-difference time-domain (3D-FDTD) method was used to simulate the electric field distributions of this structure at different wavelengths. In the simulation, we set Pd NPs and Pt NPs to have the diameters of 6 and 3.5 nm, respectively, and plane waves with transverse-electric (TE)-polarization propagating from 1 $\mu$m above the film of QNS on the glass substrate. Furthermore, we set up two detectors for the QNS: the first one is fixed in the $X$–$Y$ plane with 3 nm above the surface of glass substrate; the second one is located in the $X$–$Z$ plane at the center of 2D binary Pd–Pt QNS. These two detectors recorded the stable electric field distributions in the $X$–$Y$ and $X$–$Z$ planes of the QNS, respectively, under illumination. All of the optical constants of the materials (Pd, Pt, and glass) were obtained from the literature.[29]

Figure 8 shows the electric field distributions in the $x$–$y$ plane and $x$–$z$ plane when the plane waves (wavelengths of 365, 485, 532, 633, and 785 nm, respectively) propagated along the $z$-axis into the Pd–Pt QNS. As displayed in Figure 8a–e, the QNS provides large electric field intensities within the near field around the Pd–Pt interface, as well as the gap of composite structure in the ultraviolet (UV) (Figure 8a), visible (Figure 8b–d), and near-infrared (Figure 8e) regions. Therefore, we expected such hot spots, that is, the areas with electric field amplitudes (E2) larger than 16, to exist almost everywhere and over broad wavelengths in as-prepared Pd–Pt QNS. To verify the high density of hot spots in our Pd–Pt QNS, we collected its Raman signals in the presence of Rhodamine B (RB) ($2 \times 10^{-6}$ M) from five different positions within an area of $0.5 \times 0.5$ mm$^2$ with a spacing of 100 $\mu$m using a solid-state laser (wavelength: 532 nm) as the excitation source. Figure 8f,g shows that the Raman scattering intensities were strong and uniform even when varying the probe positions in the film of Pd–Pt QNS, which are better than those of Pd NPs or Pt NPs in previous reports.[30,31] We attribute this phenomenon to hot spots almost everywhere in the Pd–Pt QNS. Location of analytes near a hot spot would increase not only the intensities of Raman signals but also the probability to probe for the analytes. Therefore, such attractive properties of Pd–Pt QNS suggest promising applications in the surface-enhanced Raman scattering (SERS) and detection fields.

## CONCLUSION

In summary, we have developed a general approach to fabricate novel 2D QNS from self-assembly of NPs. These 2D QNS display lateral dimensions up to several micrometers and thicknesses up to a few nanometers. Moreover, these 2D QNS can be free-standing and remain intact in different solvents without any disassembly. It was demonstrated that the ligands are important factors to mediate NP assembly for formation of the 2D QNS. As a universal procedure developed in this work, a broad range of 2D unary, binary, ternary, and quaternary QNS were prepared from a variety of NPs. Co-assembly of NPs with diverse composition could bring about intriguing properties. As demonstrated in our preliminary trial with SERS, the Pd–Pt QNS have shown intensified Raman signals and are promising in detection of trace amounts of analytes. Therefore, it is anticipated that this work will open a new horizon for the exploration and design of 2D functional nanosheets by assembly technology.

## Supplementary Material

Refer to Web version on PubMed Central for supplementary material.

## ACKNOWLEDGMENTS

The authors are grateful to Dr. Kathryn Williams for her critical comments during the preparation of this manuscript. This work is supported by NIH GM R35 127130 and NSF 1645215, and by NSFC grants (NSFC 21827811 and 61527806) and the Science and Technology Project of Hunan Province (2017XK2103).

## REFERENCES

(1). Geuchies JJ; van Overbeek C; Evers WH; Goris B; de Backer A; Gantapara AP; Rabouw FT; Hilhorst J; Peters JL; Konovalov O; Petukhov AV; Dijkstra M; Siebbeles LDA; van Aert S; Bals S; Vanmaekelbergh D In Situ Study of the Formation Mechanism of Two-dimensional Superlattices from PbSe Nanocrystals. Nat. Mater 2016, 15, 1248–1254. [PubMed: 27595349]

(2). Ye X; Zhu C; Ercius P; Raja SN; He B; Jones MR; Hauwiller MR; Liu Y; Xu T; Alivisatos AP Structural Diversity in Binary Superlattices Self-Assembled from Polymer-Grafted Nanocrystals. Nat. Commun 2015, 6, 10052. [PubMed: 26628256]

(3). Lin YY; Thomas MR; Gelmi A; Leonardo V; Pashuck ET; Maynard SA; Wang Y; Stevens MM Self-Assembled 2D Free-Standing Janus Nanosheets with Single-Layer Thickness. J. Am. Chem. Soc 2017, 139, 13592–13595. [PubMed: 28902999]

(4). Smith DK; Goodfellow B; Smilgies D-M; Korgel BA Self-Assembled Simple Hexagonal $AB_2$ Binary Nanocrystal Superlattices: SEM, GISAXS, and Defects. J. Am. Chem. Soc 2009, 131, 3281–3290. [PubMed: 19216526]

(5). Evers WH; Friedrich H; Filion L; Dijkstra M; Vanmaekelbergh D Observation of a Ternary Nanocrystal Superlattice and Its Structural Characterization by Electron Tomography. Angew. Chem., Int. Ed 2009, 48, 9655–9657.

(6). Prasad BLV; Sorensen CM; Klabunde KJ Gold nanoparticle superlattices. Chem. Soc. Rev 2008, 37, 1871–1883. [PubMed: 18762836]

(7). Ho D; Sun X; Sun S Monodisperse Magnetic Nanoparticles for Theranostic Applications. Acc. Chem. Res 2011, 44, 875–882. [PubMed: 21661754]

(8). Walker DA; Browne KP; Kowalczyk B; Grzybowski BA Self-Assembly of Nanotriangle Superlattices Facilitated by Repulsive Electrostatic Interactions. Angew. Chem., Int. Ed 2010, 49, 6760–6763.

(9). Urban JJ; Talapin DV; Shevchenko EV; Kagan CR; Murray CB Synergism in Binary Nanocrystal Superlattices Leads to Enhanced p-type Conductivity in Self-assembled PbTe/Ag2Te ThinFilms. Nat. Mater 2007, 6, 115. [PubMed: 17237786]

(10). Rupich SM; Castro FC; Irvine WTM; Talapin DV Soft Epitaxy of Nanocrystal Superlattices. Nat. Commun 2014, 5, 5045. [PubMed: 25434582]

(11). Thorkelsson K; Mastroianni AJ; Ercius P; Xu T Direct Nanorod Assembly Using Block Copolymer-Based Supramolecules. Nano Lett. 2012, 12, 498–504. [PubMed: 22188307]

(12). Kim F; Kwan S; Akana J; Yang P Langmuir-Blodgett Nanorod Assembly. J. Am. Chem. Soc 2001, 123, 4360–4361. [PubMed: 11457213]

(13). Baker JL; Widmer-Cooper A; Toney MF; Geissler PL; Alivisatos AP Device-Scale Perpendicular Alignment of Colloidal Nanorods. Nano Lett. 2010, 10, 195–201. [PubMed: 19961233]

(14). Gong J; Li G; Tang Z Self-Assembly of Noble Metal Nanocrystals: Fabrication, Optical Property, and Application. Nano Today 2012, 7, 564–585.

(15). Tang Z; Zhang Z; Wang Y; Glotzer SC; Kotov NA Self-Assembly of CdTe Nanocrystals into Free-Floating Sheets. Science 2006, 314, 274–278. [PubMed: 17038616]

(16). Yang Z; Altantzis T; Zanaga D; Bals S; Tendeloo GV; Pileni M-P Supracrystalline Colloidal Eggs: Epitaxial Growth and Freestanding Three-Dimensional Supracrystals in Nanoscaled Colloidosomes. J. Am. Chem. Soc 2016, 138, 3493–3500. [PubMed: 26908091]

(17). Zhang S-Y; Regulacio MD; Han M-Y Self-Assembly of Colloidal One-dimensional Nanocrystals. Chem. Soc. Rev 2014, 43, 2301–2323. [PubMed: 24413386]

(18). Joshi RK; Schneider JJ Assembly of One Dimensional Inorganic Nanostructures into Functional 2D and 3D Architectures. Synthesis, Arrangement and Functionality. Chem. Soc. Rev 2012, 41, 5285–5312. [PubMed: 22722888]

(19). Cai R; Yang D; Yan L; Tian F; Zhang J; Lyu Y; Chen K; Hong C; Chen X; Zhao Y; Chen Z; Tan W Free-Floating 2D Nanosheets with a Superlattice Assembled from Fe3O4 Nanoparticles for Peroxidase-Mimicking Activity. ACS Appl. Nano Mater 2018, 1, 5389–5395.

(20). Silvera Batista CA; Larson RG; Kotov NA Nonadditivity of Nanoparticle Interactions. Science 2015, 350, 1242477. [PubMed: 26450215]

(21). Du Y; Yin Z; Zhu J; Huang X; Wu X-J; Zeng Z; Yan Q; Zhang H A General Method for the Large-scale Synthesis of Uniform Ultrathin Metal Sulphide Nanocrystals. Nat. Commun 2012, 3, 1177. [PubMed: 23132027]

(22). Fan H; Leve E; Gabaldon J; Wright A; Haddad RE; Brinker CJ Ordered Two- and Three-Dimensional Arrays Self-Assembled from Water-Soluble Nanocrystal-Micelles. Adv. Mater 2005, 17, 2587–2590.

(23). Zhuang J; Wu H; Yang Y; Cao YC Supercrystalline Colloidal Particles from Artificial Atoms. J. Am. Chem. Soc 2007, 129, 14166–14167. [PubMed: 17963395]

(24). Boles MA; Engel M; Talapin DV Self-Assembly of Colloidal Nanocrystals: From Intricate Structures to Functional Materials. Chem. Rev 2016, 116, 11220–11289. [PubMed: 27552640]

(25). Yang K; Peng H; Wen Y; Li N Re-examination of Characteristic FTIR Spectrum of Secondary Layer in Bilayer Oleic Acid-Coated $Fe_3O_4$ Nanoparticles. Appl. Surf. Sci 2010, 256, 3093–3097.

(26). Ji T; Lirtsman VG; Avny Y; Davidov D Preparation, Characterization, and Application of Au-Shell/Polystyrene Beads and Au-Shell/Magnetic Beads. Adv. Mater 2001, 13, 1253–1256.

(27). Zhao K; Bruinsma R; Mason TG Entropic Crystal–Crystal Transitions of Brownian Squares. Proc. Natl. Acad. Sci. U. S. A 2011, 108, 2684–2687. [PubMed: 21282614]

(28). Ye X; Millan JA; Engel M; Chen J; Diroll BT; Glotzer SC; Murray CB Shape Alloys of Nanorods and Nanospheres from Self-Assembly. Nano Lett 2013, 13, 4980–4988. [PubMed: 24044735]

(29). Palik ED Handbook of Optical Constants of Solids; Academic Press: San Diego, 1998.

(30). Chen H; Wei G; Ispas A; Hickey SG; Eychmüller A Synthesis of Palladium Nanoparticles and Their Applications for Surface-Enhanced Raman Scattering and Electrocatalysis. J. Phys. Chem. C 2010, 114, 21976–21981.

(31). Gómez R; Pérez JM; Solla-Gullón J; Montiel V; Aldaz A In Situ Surface Enhanced Raman Spectroscopy on Electrodes with Platinum and Palladium Nanoparticle Ensembles. J. Phys. Chem. B 2004, 108, 9943–9949.

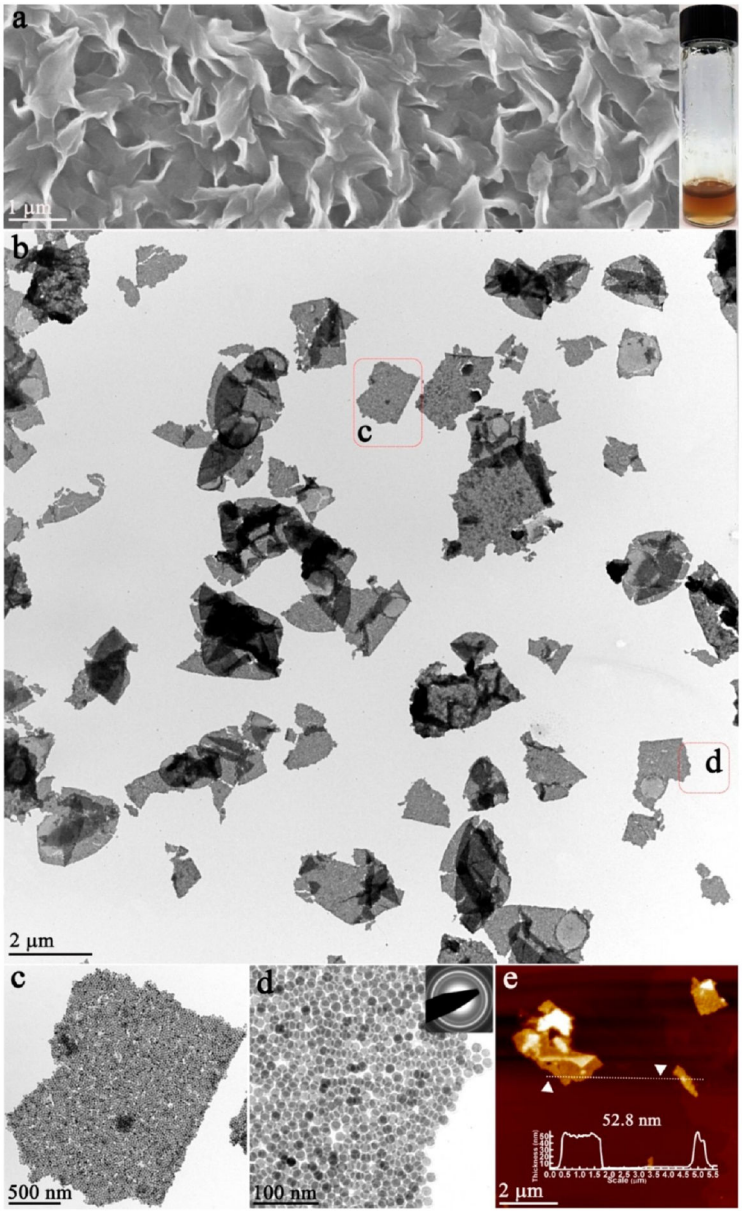


**Figure 1.**

Free-standing 2D QNS: (a) SEM image and photograph of QNS (inset); (b) low-magnification TEM image; (c) and (d) high-magnification TEM images and electron diffraction pattern (inset); (e) AFM image.

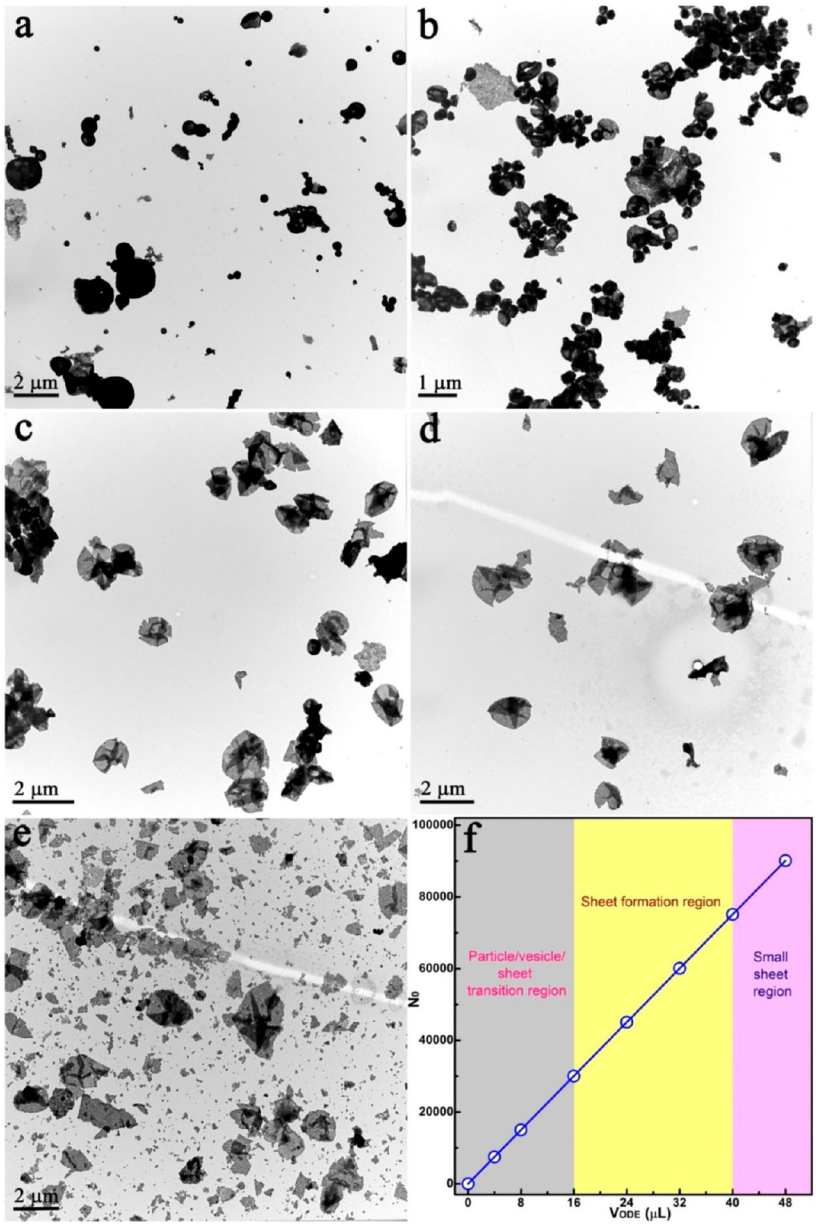


**Figure 2.**

(a–e) TEM images of the assembly process for 2D QNS. Samples prepared from NP assembly guided by different amounts of ODE: (a) 0 μL; (b) 4 μL; (c) 8 μL; (d) 24 μL; (e) 48 μL. (f) Plot of the number of ODE molecules per $Fe_3O_4$ NP.

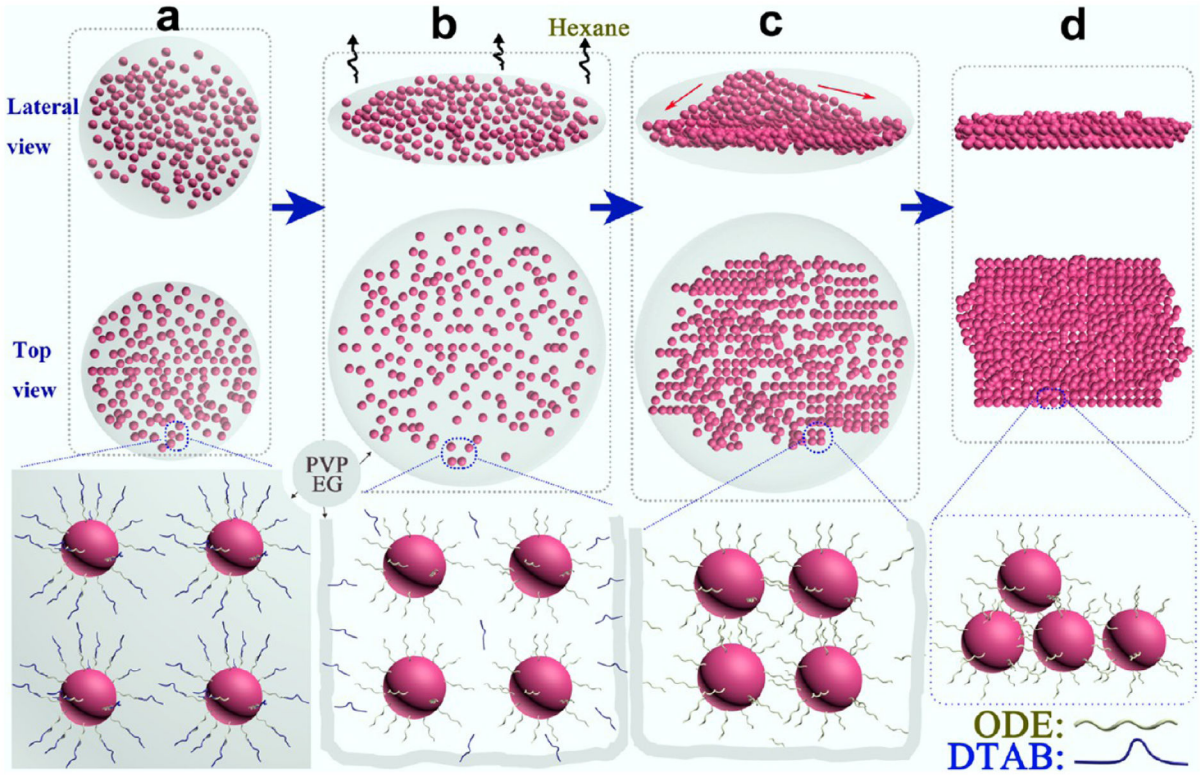


**Figure 3.**

Scheme of assembly process for 2D QNS: (a) emulsion drop casting in mixed solvent (EG and PVP); (b) hexane evaporation, self-dissociation of the DTAB layer and reformation of ODE-capping layers; (c) ODE mediates the assembly of NPs; (d) aggregated NPs extend into 2D QNS.

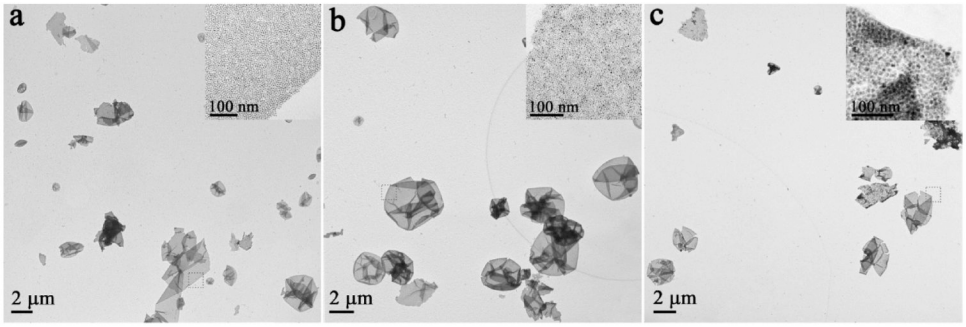


**Figure 4.**
TEM images of 2D unary QNS from the assembly of different NPs: (a) Pd QNS; (b) Pt QNS; (c) CdSe QNS.

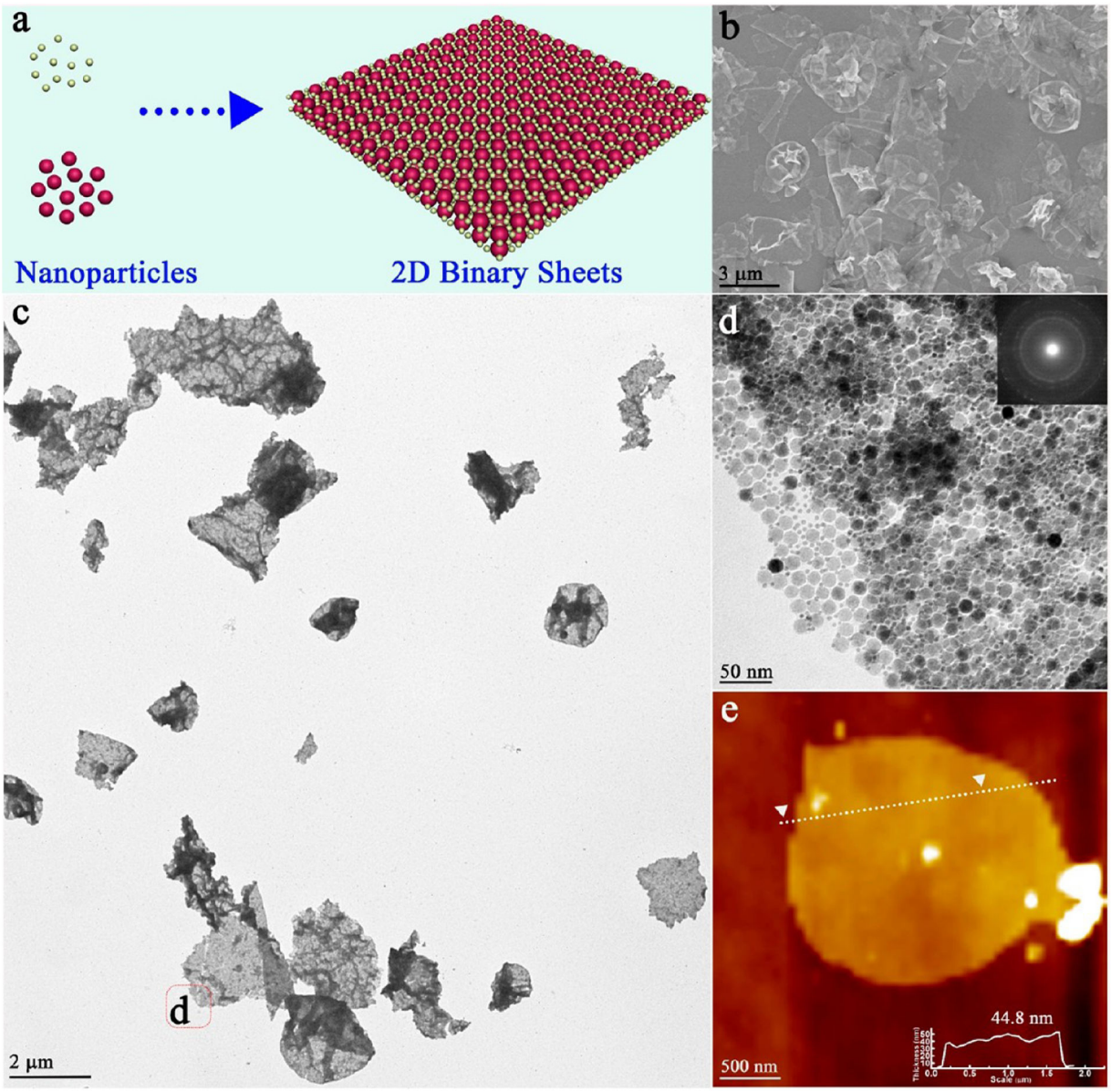


**Figure 5.**

(a) Scheme; (b) SEM image; (c) low-magnification TEM image; (d) high-magnification TEM image; (e) AFM image for 2D binary QNS from assembly of $Fe_3O_4$ NPs and Pd NPs.

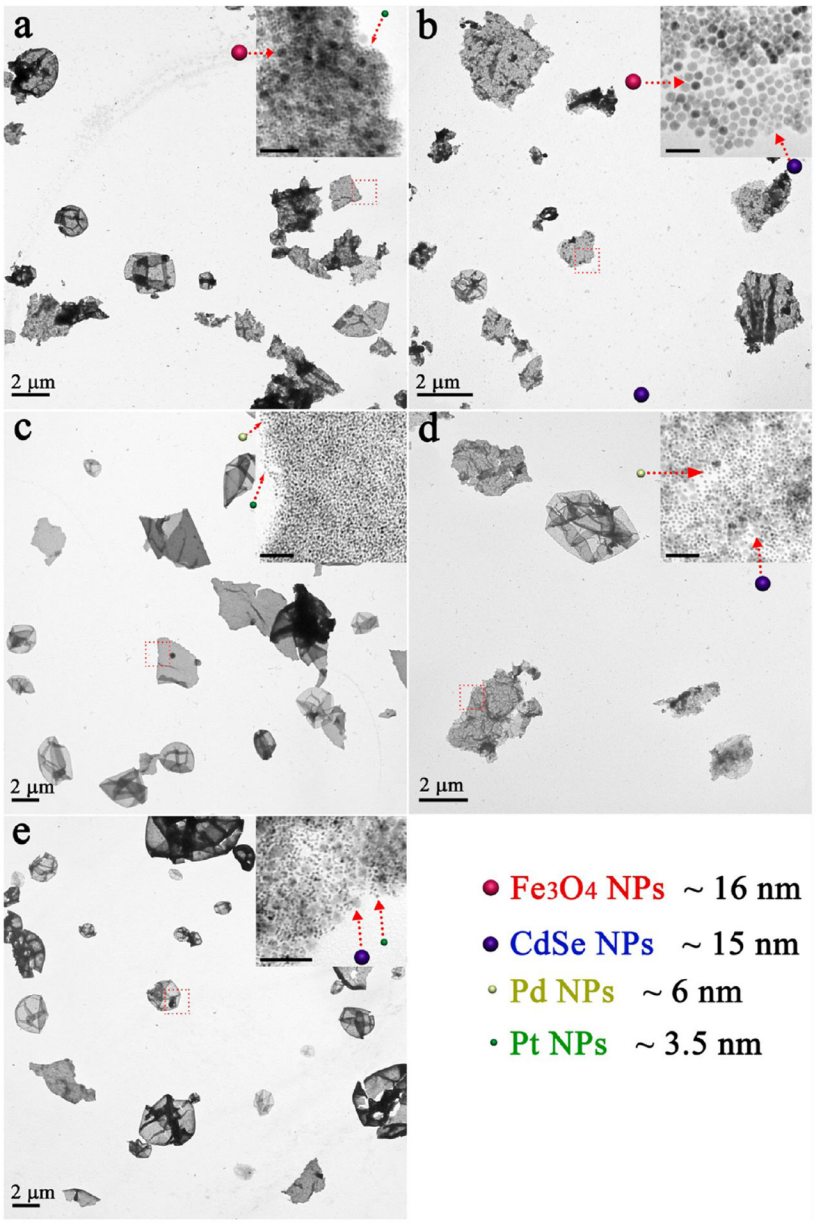


**Figure 6.**

TEM images of 2D binary QNS from assembly of two types of NPs: (a) $Fe_3O_4$–Pt QNS; (b) $Fe_3O_4$–CdSe QNS; (c) Pd–Pt QNS; (d) CdSe–Pd QNS; (e) CdSe–Pt QNS. The scales bars are 50 nm in inset images.

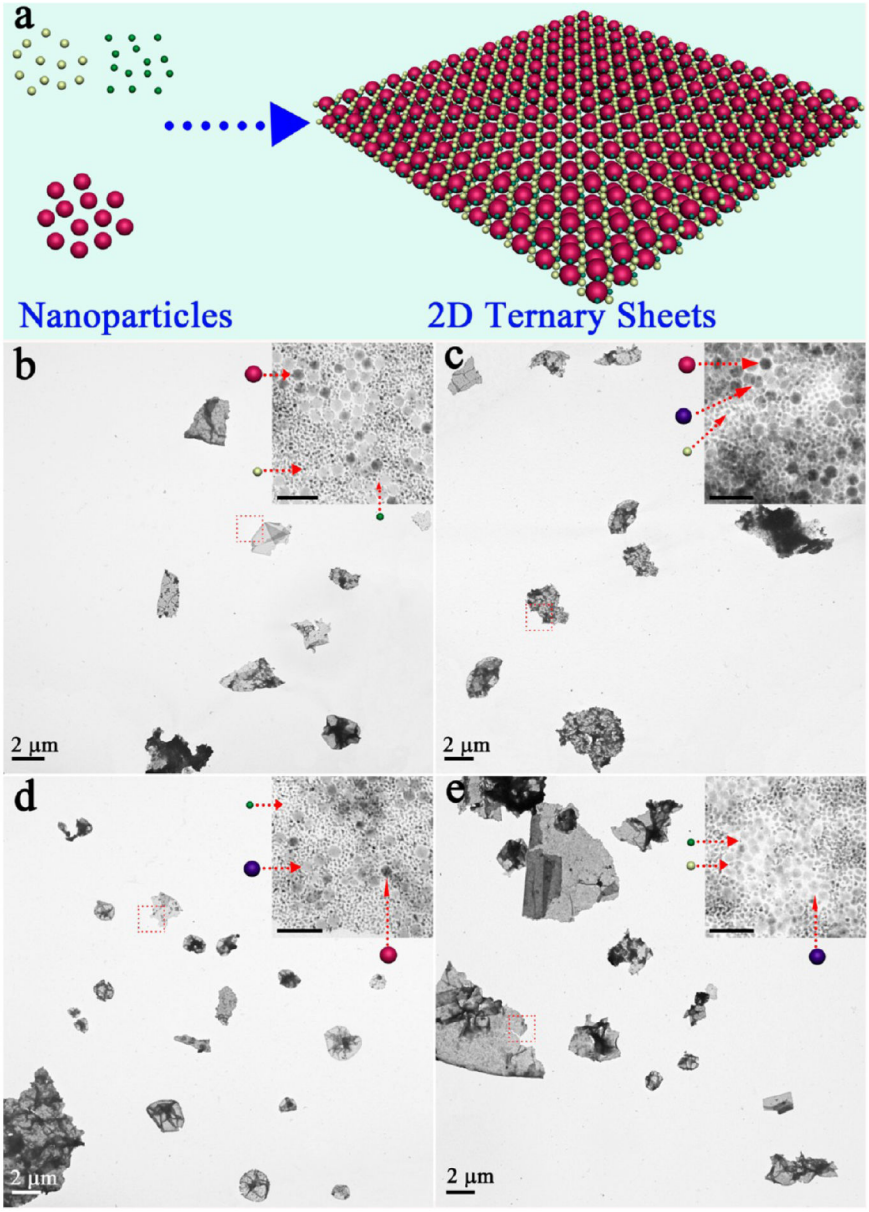


**Figure 7.**

(a) Scheme for 2D ternary QNS from assembly of three types of NPs; TEM images of 2D ternary QNS: (b) $Fe_3O_4$–Pd–Pt QNS; (c) $Fe_3O_4$–CdSe–Pd QNS; (d) $Fe_3O_4$–CdSe–Pt QNS; (e) CdSe–Pd–Pt QNS. The scale bars are 50 nm in inset images.

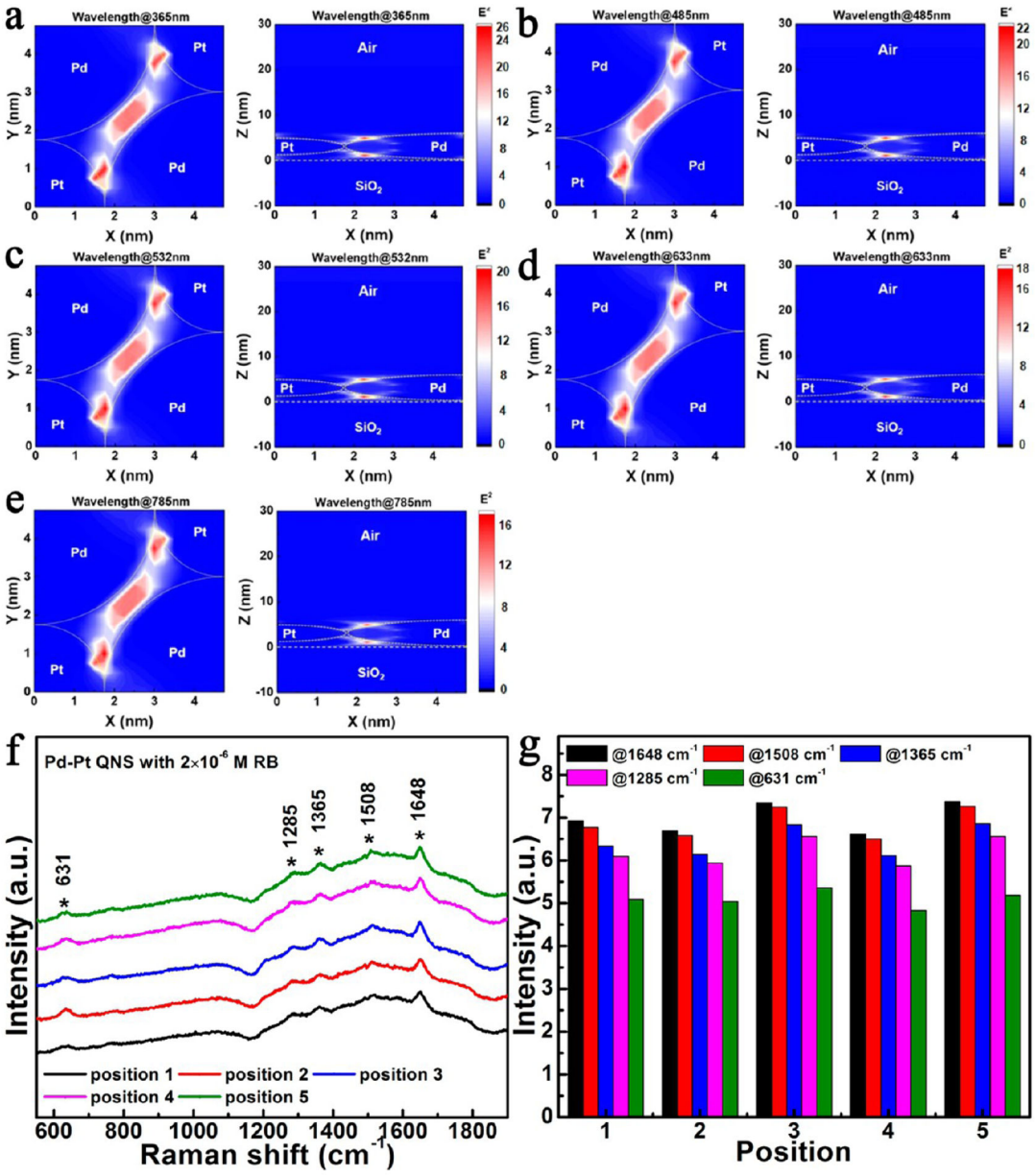


**Figure 8.**

Near-field electric field distributions of incident light at the wavelengths of (a) 365 nm, (b) 485 nm, (c) 532 nm, (d) 633 nm, and (e) 785 nm, passing through the Pd–Pt QNS on a glass substrate. Measured (f) Raman spectra and (g) Raman peak signals of Pd–Pt QNS with $2 \times 10^{-6}$ M Rhodamine B (RB), recorded at five different positions within an area of $0.5 \times 0.5$ $mm^2$ with a spacing of 100 $\mu$m.